Observation of Density-Induced Tunneling

Ole Jürgensen,[1] Florian Meinert,[2] Manfred J. Mark,[2] Hanns-Christoph Nägerl,[2] and Dirk-Sören Lühmann[1]
[1]*Institut für Laser-Physik, Universität Hamburg, Luruper Chaussee 149, 22761 Hamburg, Germany*
[2]*Institut für Experimentalphysik und Zentrum für Quantenphysik, Universität Innsbruck, 6020 Innsbruck, Austria*
(Received 3 July 2014; published 7 November 2014)

We study the dynamics of bosonic atoms in a tilted one-dimensional optical lattice and report on the first direct observation of density-induced tunneling. We show that the interaction affects the time evolution of the doublon oscillation via density-induced tunneling and pinpoint its density and interaction dependence. The experimental data for different lattice depths are in good agreement with our theoretical model. Furthermore, resonances caused by second-order tunneling processes are studied, where the density-induced tunneling breaks the symmetric behavior for attractive and repulsive interactions predicted by the Hubbard model.

DOI: 10.1103/PhysRevLett.113.193003 PACS numbers: 37.10.Jk, 03.75.Lm, 67.85.Hj, 75.10.Pq

The Hubbard model is the primary description for strongly correlated electrons in solids. It takes into account the interaction between the particles at a lattice site and the tunneling between the sites, whereas other interaction processes are neglected. It was pointed out that these additional interactions may have a crucial influence on strongly correlated materials such as superconductors or ferromagnets [1–4]. Of particular importance is the so-called bond-charge interaction that represents a density-induced tunneling of an electron. In solids, this interaction-driven process cannot be studied systematically due to the lack of direct control over the electron density and the interaction strength. Furthermore, the complexity of the investigated materials hinders a direct observation of this interaction effect. Hence, the role of interaction-induced tunneling has remained an open question in condensed matter physics.

Ultracold atoms in optical lattices allow the realization of extremely pure lattice systems without defects and phononic excitations. Furthermore, the unique control of both the lattice potential and the interaction strength permits a systematic study of static and dynamic properties. In optical lattices, density-induced tunneling [5–9] is even more pronounced due to the characteristic shape of the Wannier functions [7]. Several indications for density-induced tunneling have been found: It has a strong influence on the superfluid to Mott-insulator transition in bosonic [7,10,11] and multicomponent systems such as Bose-Fermi mixtures of atoms [6,8,12–15]. As a tunneling process, it also modifies the effective band structure, which has also been observed in a Bose-Fermi mixture [16]. A direct observation of density-induced tunneling processes was hindered mainly by the fact that the Mott insulator transition depends only on the ratio of on-site interaction and total tunneling and by the averaging over different on-site occupancies in experimental systems.

Here, we report on the direct observation of density-induced tunneling with ultracold atoms in a tilted one-dimensional optical lattice. We study the dynamics of a 1D Mott insulator after quenching the tilt energy E between neighboring sites into resonance with the on-site interaction energy U. We show that the resulting resonant particle oscillation between neighboring sites (see inset of Fig. 1) is driven by interaction-induced tunneling on top of conventional tunneling. The experimental control over the on-site occupancy and the interaction strength via a Feshbach resonance [11] allows us to isolate the effect of interaction-induced tunneling and to study it systematically.

The observed oscillation frequency f_0 is expected to be directly proportional to the tunneling matrix element J and is plotted in Fig. 1 as a function of the atomic scattering length a_s. The plot shows that the tunneling rate is modified by the interaction strength and the density of the sample. The Hubbard model predicts a constant value for J (dashed lines in Fig. 1). In contrast, density-induced tunneling ΔJ

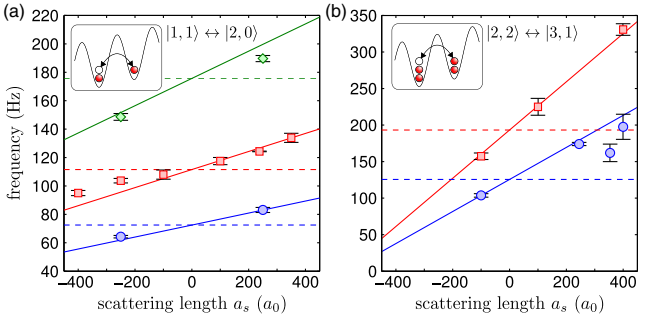

FIG. 1 (color online). Oscillation frequency f_0 of the doublon number in a tilted lattice as a function of a_s for $V_z = 8E_R$ (diamonds), $10E_R$ (squares), and $12E_R$ (circles) with initial on-site occupancy (a) $n = 1$ and (b) $n = 2$ (see insets). The dashed lines show the prediction of the standard Hubbard model. The solid lines depict the interaction dependence due to density-induced tunneling [see Eq. (1)]. Theoretical predictions correspond to a 4% lower lattice depth [17]. The experimental data of (a) are taken from Ref. [18].

changes linearly with a_s and the on-site occupancy n, contributing to the total tunneling energy via

$$J_{\mathrm{tot}} = J + (n_i + n_j - 1)a_s \Delta J, \tag{1}$$

for a tunneling process involving neighboring sites i and j. The measured oscillation frequency agrees very well with this modified tunneling rate (solid lines in Fig. 1). Increasing the on-site occupation from $n = 1$ to $n = 2$ enhances the slope of the experimental data in accordance with Eq. (1). This allows us to identify the density-induced tunneling process unambiguously and shows that its amplitude can even be as strong as that of conventional tunneling.

The experiments are performed as reported in detail in Ref. [18]. Starting from a Cs Bose-Einstein condensate, we prepare a bosonic Mott insulator in a 3D cubic optical lattice with a lattice depth $V_q = 20E_R$ $(q = x, y, z)$, where $E_R = h \times 1.325$ kHz denotes the photon recoil energy, and h is Planck's constant [17]. Adjusting initial density, interactions, and external confinement during lattice loading allows us to prepare either a clean one-atom- or a two-atom-per-site Mott shell [17]. We set a_s to the desired value $(-400a_0 \leq a_s \leq +400a_0)$ by means of a Feshbach resonance. Tunneling dynamics along 1D chains is initiated by first setting the tilt E along the vertical z direction via a magnetic force $|\nabla B|$ and then quickly lowering V_z along the direction of the tilt. We measure the number of doubly occupied sites (doublons) after a variable evolution time t_h through Feshbach molecule formation and detection [18]. On resonance $(E \approx U)$ the doublon number exhibits large-amplitude oscillations. For $n = 1$ the oscillation frequency f_0 is deduced from a damped sinusoidal fit to the data [18]. In Fig. 1(a) we give f_0 as a function of a_s for three different V_z from data sets taken for Ref. [18]. Time traces for $n = 2$ need a more refined spectral analysis (see below). Figure 1(b) plots the (mean) frequency deduced from measurements with $n = 2$ as a function of a_s for $V_z = 10E_R$ and $V_z = 12E_R$. The observed frequencies clearly depend on both the interaction strength a_s and the on-site occupancy n in the lattice. The Hubbard model (dashed lines) predicts constant J, which solely depends on the lattice depth V_z [19], and cannot reproduce this behavior.

For the theoretical description of the experiment we make use of the generalized Hubbard Hamiltonian for the one-dimensional lattice including density-induced tunneling, which is given by

$$\hat{H} = -J\sum_i \hat{b}_i^\dagger \hat{b}_{i+1} + \mathrm{c.c.} + \frac{U}{2}\sum_i \hat{n}_i(\hat{n}_i - 1) + E\sum_i \hat{n}_i i - a_s \Delta J \sum_i \hat{b}_i^\dagger (\hat{n}_i + \hat{n}_{i+1})\hat{b}_{i+1} + \mathrm{c.c.} \tag{2}$$

with the tunneling matrix element J, the on-site interaction U, a tilt E per lattice site, bosonic annihilation (creation) operators $\hat{b}_i^{(\dagger)}$ on site i, and $\hat{n}_i = \hat{b}_i^\dagger \hat{b}_i$. The first line is the standard Bose-Hubbard model, whereas the second line represents the density-induced tunneling operator. It originates from the two-body interaction operator and represents the dominant off-site contribution for neutral atoms in optical lattices [7–9]. Its amplitude,

$$\Delta J = -\frac{4\pi\hbar^2}{m}\int d^3 r w^*(\mathbf{r} - \mathbf{d}) w^*(\mathbf{r}) w^2(\mathbf{r}), \tag{3}$$

is determined by the Wannier functions $w(\mathbf{r})$ of the lowest band of the lattice with the lattice spacing d using a δ-shaped interaction potential. This tunneling operator is explicitly occupation dependent due to the factor $(\hat{n}_i + \hat{n}_{i+1})$. Assuming that the time evolution on neighboring sites is predominantly given by a constant total occupation $n_i + n_{i+1} = 2n$, we can define an effective total tunneling operator as

$$\hat{J}_{\mathrm{tot}} = -J_{\mathrm{tot}} \sum_i \hat{b}_i^\dagger \hat{b}_{i+1} + \mathrm{c.c.} \tag{4}$$

using Eq. (1), which allows us to retrieve the standard Bose-Hubbard model with a modified tunneling rate J_{tot}.

It is *a priori* not clear that conventional and density-induced tunneling can be combined to one total hopping process. To verify this simplification, we perform exact numerical simulations of the time evolution of the initial state by diagonalizing the generalized Hubbard model (2) for a finite lattice with $N = 8$ sites. Using the exact solution, we are not restricted to short time traces, allowing us to resolve the full Fourier spectrum. We first discuss the case of an initial on-site occupation $n = 1$. As an example, the insets in Fig. 2(a) show time traces of the number of doublons $(n_i = 2)$ for $V_z = 10E_R$ and $a_s = 400a_0$ at the resonance $E = U$. Here, the number of triply occupied sites (triplons) is negligible. The Fourier spectrum [Fig. 2(a)] contains a broad range of frequencies that are peaked around $f_0 = \nu J_{\mathrm{tot}}/h$ (bottom) or around $f_0 = \nu J/h$ (top) for the standard Hubbard model $(\Delta J = 0)$ with the prefactor $\nu \approx 4$, as indicated by the vertical lines. By means of time-dependent DMRG of up to 40 sites, it has been shown in Ref. [18] that the system size does not significantly affect the characteristic oscillation frequency f_0 for Mott chains beyond 3 sites but causes increased many-body damping with increasing system size (see also [17]).

In Fig. 2(b), the frequency spectrum is plotted against the bare tunneling rate J/h for the generalized Hubbard model $(\Delta J \neq 0)$. The centroid of the two strongest modes matches with the total tunneling rate $4J_{\mathrm{tot}}/h$, while the dashed line corresponds to the standard Hubbard model with $4J/h$. Plotted as a function of the scattering length a_s [Fig. 2(c)], the difference between standard and generalized Hubbard model becomes even more obvious. As the absolute value of the on-site interaction is compensated by the resonance condition $E = U$, the doublon dynamics is independent of

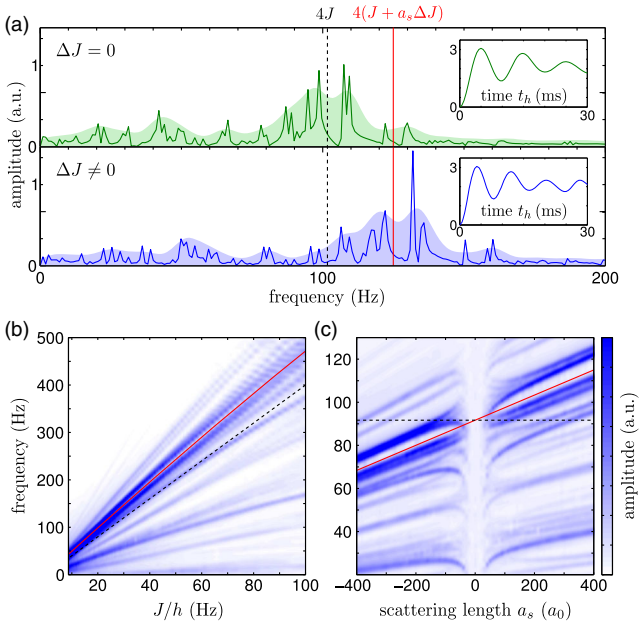

FIG. 2 (color online). (a) Fourier spectrum of the simulated doublon number dynamics for $E = U$ without (upper panel) and with (lower panel) inclusion of density-induced tunneling. Here, $n = 1$, $V_z = 10E_R$, and $a_s = 400a_0$. The dashed (solid) line shows the predominant frequency component predicted without (with) density-induced tunneling. The shaded areas incorporate a Gaussian broadening with a width $w = 4$ Hz for visualization purposes. The insets show the time trace for the first 30 ms. (b) Mode spectrum as a function of the single-particle tunneling rate J/h tuned via the lattice depth V_z for $a_s = 400a_0$ ($w = 4$ Hz). (c) Mode spectrum as a function of a_s at fixed $V_z = 10E_R$ ($w = 1$ Hz). In (b) and (c) the dashed line shows $4J/h$, while the solid line shows $4J_{\mathrm{tot}}/h$, including density-induced tunneling.

a_s within the standard Hubbard model (dashed line). In contrast, the interaction dependence of density-induced tunneling imprints a linear dependence on the observed frequency modes $f_0 \propto J + a_s\Delta J$.

Although the theoretical spectrum of the time evolution contains several distinct features, we can conclude that the main frequency can be attributed to an oscillation with $4J_{\mathrm{tot}}/h$. Fitting the experimental time traces for $n = 1$ with a damped oscillation [18] allows us to extract this central frequency plotted in Fig. 1(a). The experimental data points pinpoint the dependence on the interaction strength as discussed above and agree well with the generalized model including density-induced tunneling. Note that the interaction-induced admixture of higher bands will lead to a slightly modified rate for the total tunneling [7–9,20].

Let us now turn to the direct verification of the density dependence of the interaction-driven tunneling process by preparing an initial state with on-site occupancy $n = 2$. Because of $J_{\mathrm{tot}} = (2n-1)a_s\Delta J$, the impact of the density-induced tunneling is expected to increase by a factor of 3. In Fig. 3(a) we plot the number of doubly and singly occupied sites as a function of E measured after $t_h = 50$ ms for two different values of U. Close to the expected resonance position at $E = U$, we observe two minima in the doublon number [Fig. 3(a)] that can be attributed to the processes $|2,2\rangle \leftrightarrow |3,1\rangle$ and $|2,0\rangle \leftrightarrow |1,1\rangle$. The latter arises from tunneling at residual defects (empty sites) in the $n = 2$ shell [17]. The splitting of the resonance arises from corrections to the on-site energy U due to multiorbital effects [7,11,21–23] causing an intrinsically occupation dependent on-site energy U_n. While for the defect process $|2,0\rangle \leftrightarrow |1,1\rangle$ the resonance is at $E_{11} = U_2$, the process $|2,2\rangle \leftrightarrow |3,1\rangle$ is resonant at $E_{22} = 3U_3 - 2U_2 < U_2$.

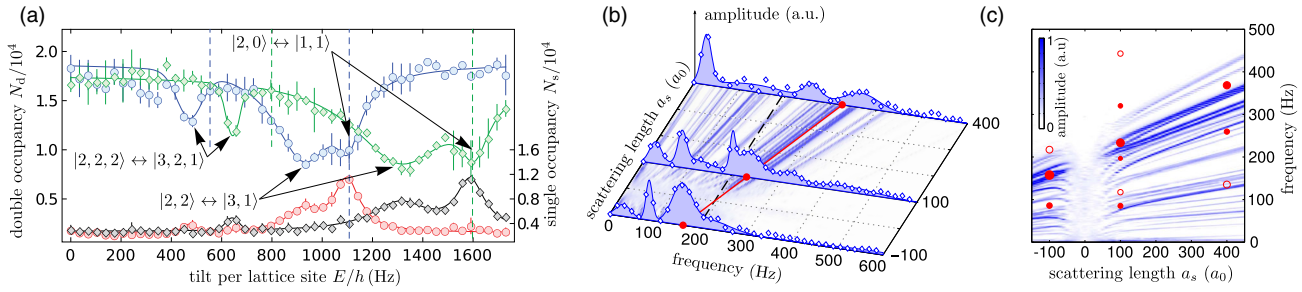

FIG. 3 (color online). Doublon dynamics for on-site occupancy $n = 2$. (a) Number of doubly (upper lines) and singly (lower lines) occupied sites as a function of E after $t_h = 50$ ms for $a_s = 245(5)a_0$ (circles) and $a_s = 354(5)a_0$ (diamonds) at $V_z = 12E_R$, giving resonances for the $|2,2\rangle \leftrightarrow |3,1\rangle$ oscillations at $E_{22} = h \times 940(20)$ Hz and $E_{22} = h \times 1283(20)$ Hz, respectively (see [17] for details). The dashed lines indicate the calculated U and $U/2$. (b) Measured Fourier spectra extracted from time traces of the doublon number at $V_z = 10E_R$ and $E = E_{22}$ for different a_s. The solid blue lines result from multiple Gaussians fits to the data [17]. The shaded area projected into the axis plane depicts the simulated Fourier spectra shown in (c). The lines show the expected frequencies for the standard (dashed) and extended (solid) Hubbard model [Eq. (1)]. (c) Simulated Fourier spectra as a function of a_s incorporating a Gaussian broadening with a width $w = 1$ Hz. The markers denote peak positions deduced from the experimental data shown in (b). The marker size scales linearly with the area under the respective fits. Open circles indicate broad Gaussian fits with a large ratio of width and amplitude $w/A > 0.2$.

The resonances at $E_{22}/2$ correspond to the second-order tunneling process $|2,2,2\rangle \leftrightarrow |3,2,1\rangle$. Second-order tunneling to hole defects $|2,2,0\rangle \leftrightarrow |1,2,1\rangle$ at $E_{11}/2$ does not contribute, since the intermediate state $|1,3,0\rangle$ is strongly off resonant. For the measurement of the time traces we determine E_{22} for a fixed lattice depth and scattering length. Since the two resonances at E_{11} and E_{22} are not fully separated, we expect (off-resonant) contributions from defect sites to contribute with up-shifted frequencies [18].

In Fig. 3(b) Fourier spectra extracted from the experimental time traces [17] are shown for three different values of a_s in the range $-100a_0 \leq a_s \leq +400a_0$. We obtain the main frequency modes using Gaussian fits (blue areas). While the lowest observable frequency is caused by decoherence and particle loss, we can identify the dominant mode at the expected position $f_0 = \nu(J + 3a_s\Delta J)$ (red solid line), with $\nu = 4\sqrt{3}$ for the $|2,2\rangle \leftrightarrow |3,1\rangle$ process. For the two positive values of a_s, where the frequency range leads to better resolved peaks, a splitting of this mode can be observed. This splitting is in general also visible in the theoretical spectrum in Fig. 3(c), where the circles denote the experimentally extracted modes. Moreover, we can identify a mode with lower frequencies that could probably be assigned to the mode around $\nu \approx 3\sqrt{3}/2$ in the numerical spectrum. However, defect sites will effectively lead to decoupled chains with different lengths surrounded by unoccupied sites affecting the prefactor ν.

The extracted dominant frequencies are plotted for $V_z = 10E_R$ and $V_z = 12E_R$ [17] in Fig. 1(b), where we use the centroid for split resonances. For both lattice depths, we see a good agreement with the theoretical expectation $f_0 = 4\sqrt{3}(J + 3a_s\Delta J)$. In combination with results for $n = 1$, this serves as direct confirmation of the density dependence of the tunneling.

As has been demonstrated recently [24], the dynamics in tilted lattices also allows the study of higher-order tunneling processes. In Fig. 4(a), the numerically determined doublon number, averaged over the time evolution, is plotted as a function of E, depicting several distinct resonances at fractional values of U in accordance with the experimental observation in Ref. [24]. The resonance at $E = U/2$ is caused by second-order tunneling processes via an intermediate site. In this case, the hopping to next-nearest neighbor sites restores the resonant tunneling condition ($2E = U$), whereas direct nearest-neighbor tunneling is suppressed. Higher-order resonances at $E = U/n$ are caused by long-range tunneling processes proportional to $J(J/U)^{n-1}$. Density-induced tunneling causes a broadening of the resonances for repulsive interactions (blue line) and a narrowing for attractive interactions (red line).

The numerical Fourier spectrum for the resonant second-order tunneling dynamics is plotted in Fig. 4(b). A clear evidence for the impact of density-induced tunneling is the breaking of the symmetry between attractive and repulsive interaction [17,25], which holds for the Hubbard model,

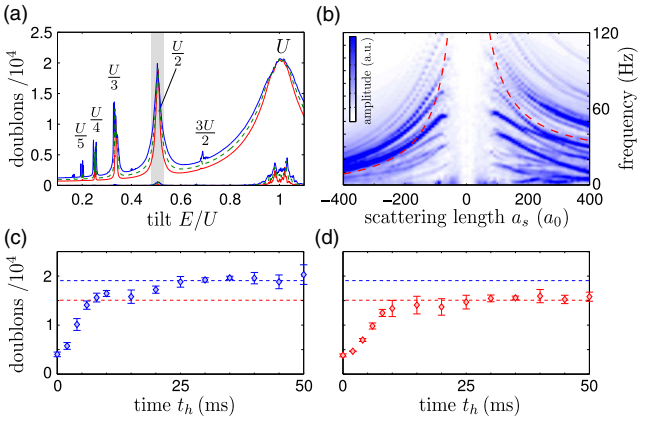

FIG. 4 (color online). (a) Time-averaged number of the sum of doublons and triplons (upper lines) and triplons only (lower lines) as a function of E for $V_z = 8E_R$ at $a_s = 250a_0$ (blue) and $a_s = -250a_0$ (red). The solid lines show numerical simulations including density-induced tunneling, while for the dashed lines $\Delta J = 0$. The gray area indicates sampling over E in the experiment with an estimated width of ≈50 Hz. (b) Numerical Fourier spectrum of the doublon dynamics as a function of a_s revealing the breaking of symmetry between attractive and repulsive scattering for $E = U/2$. The dashed line indicates $f_0 = \nu(J + a_s\Delta J)(J + 2a_s\Delta J)/U$ with a prefactor $\nu = 19$ in accordance with [24]. Experimental time traces at the $U/2$ resonance for (c) $a_s = +250a_0$ and (d) $a_s = -250a_0$ at $V_z = 8E_R$ showing an asymmetric behavior between repulsive and attractive interaction caused by density-induced tunneling. The dashed lines are guides to the eye that indicate the steady-state doublon number.

i.e., $\Delta J = 0$. This frequency shift can also be observed in the experimental time traces in Figs. 4(c) and 4(d), where the faster initial increase for repulsive interactions indicates a higher frequency. In addition, we find a decrease in the average doublon number for attractive interactions, which we attribute to the reduced width of the second-order tunneling resonance [see Fig. 4(a)], as the variation of E across the sample due to the small residual harmonic confinement and a variation in a_s due to the magnetic field gradient (gray area) is comparable with the resonance width.

We have presented the first direct measurement of density-induced tunneling of ultracold atoms in optical lattices. We observe resonant doublon dynamics when compensating the interaction energy U by an applied tilt. The measured frequency exhibits a linear dependence on the on-site occupancy and on the scattering length. Our numerical simulations show that an extended Hubbard model incorporating the density-induced tunneling accurately describes the experiment. For approximately constant densities both tunneling processes can be described with a single effective amplitude $J + (2n-1)a_s\Delta J$ that can differ strongly from the conventional tunneling J. Furthermore, we have studied second-order tunneling processes and observe an asymmetry between repulsive and attractive interactions caused by density-induced

tunneling. This underlines its importance for exchange interactions that are, e.g., responsible for antiferromagnetic properties in solids [26]. Our results grant future perspectives for detailed investigations of complex interaction effects caused, e.g., by higher orbitals and off-site interactions [7,20].

We are indebted to R. Grimm for generous support, and thank A. Daley for fruitful discussions. We gratefully acknowledge funding by the Deutsche Forschungsgemeinschaft (Grants No. SFB 925 and No. GRK 1355) and the European Research Council (ERC) under Project No. 278417.

[1] J. E. Hirsch, Physica (Amsterdam) **158C**, 326 (1989).
[2] R. Strack and D. Vollhardt, Phys. Rev. Lett. **70**, 2637 (1993).
[3] J. E. Hirsch, Physica (Amsterdam) **199–200B**, 366 (1994).
[4] J. C. Amadon and J. E. Hirsch, Phys. Rev. B **54**, 6364 (1996).
[5] G. Mazzarella, S. M. Giampaolo, and F. Illuminati, Phys. Rev. A **73**, 013625 (2006).
[6] A. Mering and M. Fleischhauer, Phys. Rev. A **83**, 063630 (2011).
[7] D.-S. Lühmann, O. Jürgensen, and K. Sengstock, New J. Phys. **14**, 033021 (2012).
[8] O. Jürgensen, K. Sengstock, and D.-S. Lühmann, Phys. Rev. A **86**, 043623 (2012).
[9] O. Dutta, M. Gajda, P. Hauke, M. Lewenstein, D.-S. Lühmann, B. A. Malomed, T. Sowiński, and J. Zakrzewski, arXiv:1406.0181.
[10] S. Pilati and M. Troyer, Phys. Rev. Lett. **108**, 155301 (2012).
[11] M. J. Mark, E. Haller, K. Lauber, J. G. Danzl, A. J. Daley, and H.-C. Nägerl, Phys. Rev. Lett. **107**, 175301 (2011).
[12] S. Ospelkaus, C. Ospelkaus, O. Wille, M. Succo, P. Ernst, K. Sengstock, and K. Bongs, Phys. Rev. Lett. **96**, 180403 (2006).
[13] K. Günter, T. Stöferle, H. Moritz, M. Köhl, and T. Esslinger, Phys. Rev. Lett. **96**, 180402 (2006).
[14] T. Best, S. Will, U. Schneider, L. Hackermüller, D. van Oosten, I. Bloch, and D.-S. Lühmann, Phys. Rev. Lett. **102**, 030408 (2009).
[15] D.-S. Lühmann, K. Bongs, K. Sengstock, and D. Pfannkuche, Phys. Rev. Lett. **101**, 050402 (2008).
[16] J. Heinze, S. Götze, J. S. Krauser, B. Hundt, N. Fläschner, D.-S. Lühmann, C. Becker, and K. Sengstock, Phys. Rev. Lett. **107**, 135303 (2011).
[17] See Supplemental Material at http://link.aps.org/supplemental/10.1103/PhysRevLett.113.193003 for details on experimental preparation, error bars, and Fourier analysis.
[18] F. Meinert, M. J. Mark, E. Kirilov, K. Lauber, P. Weinmann, A. J. Daley, and H.-C. Nägerl, Phys. Rev. Lett. **111**, 053003 (2013).
[19] D. Jaksch, C. Bruder, J. I. Cirac, C. W. Gardiner, and P. Zoller, Phys. Rev. Lett. **81**, 3108 (1998).
[20] U. Bissbort, F. Deuretzbacher, and W. Hofstetter, Phys. Rev. A **86**, 023617 (2012).
[21] H. P. Büchler, Phys. Rev. Lett. **104**, 090402 (2010).
[22] S. Will, T. Best, U. Schneider, L. Hackermüller, D.-S. Lühmann, and I. Bloch, Nature (London) **465**, 197 (2010).
[23] M. J. Mark, E. Haller, K. Lauber, J. G. Danzl, A. Janisch, H. P. Büchler, A. J. Daley, and H.-C. Nägerl, Phys. Rev. Lett. **108**, 215302 (2012).
[24] F. Meinert, M. J. Mark, E. Kirilov, K. Lauber, P. Weinmann, M. Gröbner, A. J. Daley, and H.-C. Nägerl, Science **344**, 1259 (2014).
[25] K. Sakmann, A. I. Streltsov, O. E. Alon, and L. S. Cederbaum, Phys. Rev. A **82**, 013620 (2010).
[26] P. Anderson, Phys. Rev. **79**, 350 (1950).